FINITE ELEMENT SIMULATION OF THE MECHANICALLY COUPLED COOK OFF EXPERIMENT FOR HIGH EXPLOSIVES

J.M. Gerken[*], J.G. Bennett[*], and F.W. Smith[†]

This paper develops and applies a method to model dynamic crack propagation in structures. The technique is developed via the three field Hu-Washizu Energy Principle for the implicit finite element method. This method is then incorporated into simulation of an experiment called the Mechanically Coupled Cook Off (MCCO) experiment in which a confined sample of polymer bonded explosive is heated and then ignited. High-speed photographs of the experiment show a pattern of cracks propagating through the explosive. The results of the numerical simulation show that the general features of the experiment are reproduced.

INTRODUCTION

There has been considerable interest in developing numerical models having the capability to predict the structural static and dynamic response of structures in the presence of failure by fracture. There are several challenges that must be addressed in modeling of dynamic crack propagation. Primary among these challenges are producing the correct material behavior in the presence of fracture and modeling geometry changes that are a result of crack propagation. Previous and ongoing efforts to model fracture in structures include most, if not all, of the well developed computational methods (Liebowitz et al. [1] and Aliabadi [2]). In reviews given by Nishioka [3] and De Borst [4], among others, it can be seen that much of this effort has been dedicated to fracture modeling using the finite element method. Some of the techniques employed include special element formulation to model crack tip singularities and discontinuities (e.g. Banks-Sills and Sherman [5], and Lotfi and Shing, [6]), adaptive meshing (e.g. Nishioka et al. [7]), fracture parameter calculation (e.g. Li et al. [8], and Parks [9]), damage evolution (e.g. Lemaitre [10]) and discrete fracture models (e.g. Hoff et al. [11], Liaw et al. [12], and Xu and Needleman, [13]). While these methods provide valuable computational abilities with specific applications, the main goal of this work is to provide an accurate fracture model that is comparable in complexity and application to current structural finite element simulations.

[*]Los Alamos National Laboratory, ESA-EA MS P946, Los Alamos, New Mexico 87545, USA

[†]Colorado State University, Department of Mechanical Engineering

This paper presents an implicit finite element method, developed by Gerken [14], that models discrete fracture in two-dimensional structures and addresses the primary challenges of discrete fracture modeling. The method incorporates discrete fracture by allowing the propagation of cracks along pre-existing element interfaces. The approach to developing such a method is to first develop a 2 dimensional finite element from the Hu-Washizu Energy Principle, which has a small, "virtual", crack on its edge. The finite element mesh then contains a virtual crack at each element interface along which discrete cracks can propagate. The analysis is formulated on the element level and the implicit finite element code ABAQUS/Standard [15] is used to enforce the boundary conditions, assemble the global equations and solve for the nodal variables.

This method is then used in a finite element model of the Mechanically Coupled Cook Off (MCCO) of High Explosives Experiment. The MCCO experiment is one in which the "cook-off" of a plastic bonded explosive material is produced by confining a thick circular ring of the explosive material in a thin circular metal ring and then subjecting the assembly to a uniform temperature increase. After the explosive becomes highly reactive, several optical photographs of the explosive are recorded. One of the phenomenon observed in the photographs is 3 to 5 distinct narrow zones of luminous activity propagate from the inner surface of the explosive ring outward towards the confinement ring. These luminous zones are postulated to be the ignition of newly exposed surface as discrete cracks propagate through the explosive.

The remainder of this paper will present a detailed development of the discrete fracture model and its application in the finite element simulation of the MCCO experiment. In the results section it is shown that by introduction of a size distribution of initial "virtual" cracks, both the mechanical and temporal features of the experiment are reproduced.

FINITE ELEMENT EQUATIONS

The Hu-Washizu Energy Principle is a three-field principle in which the displacement, strain and stress fields are independent. Following that of Weissman and Taylor [16], the Hu-Washizu Principle is stated as

$$\Pi_{HW}\left(\mathbf{u},\boldsymbol{\sigma},\boldsymbol{\varepsilon}\right)=\int_{\Omega}\left[\frac{1}{2}\boldsymbol{\varepsilon}^{\mathrm{T}}\mathbf{D}\boldsymbol{\varepsilon}-\boldsymbol{\varepsilon}^{\mathrm{T}}\mathbf{D}\boldsymbol{\varepsilon}_{0}+\boldsymbol{\varepsilon}^{\mathrm{T}}\boldsymbol{\sigma}_{0}+\boldsymbol{\sigma}^{\mathrm{T}}\left(\mathbf{L}\mathbf{u}-\boldsymbol{\varepsilon}\right)\right]\mathrm{d}\Omega-\Pi_{\mathrm{EXT}} \qquad (1)$$

where Ω is the volume, $\mathbf{u}$, $\boldsymbol{\sigma}$, and $\boldsymbol{\varepsilon}$ are the displacement stress and strain fields respectively, $\mathbf{D}$ is the elastic moduli coefficients matrix, $\boldsymbol{\varepsilon}_0$ and $\boldsymbol{\sigma}_0$ are the initial strain and stress tensors respectively, Π_{EXT} is the external work, and $\mathbf{L}$ is the strain displacement operator.

Then, taking the first variation of eqn. (1) and equating it to zero,

$$\int_{\Omega}\left[\delta\boldsymbol{\sigma}^{T}\left(\mathbf{L}\mathbf{u}-\boldsymbol{\varepsilon}-\boldsymbol{\varepsilon}^{a}\right)+\delta\boldsymbol{\varepsilon}^{T}\left(\mathbf{D}\boldsymbol{\varepsilon}-\mathbf{D}\boldsymbol{\varepsilon}_{0}+\boldsymbol{\sigma}_{0}-\boldsymbol{\sigma}\right)+\delta\mathbf{u}^{T}\left(\mathbf{L}^{T}\boldsymbol{\sigma}-\mathbf{b}\right)\right]d\Omega-\int_{\Gamma_{\sigma}}\delta\mathbf{u}^{T}\mathbf{t}^{a}d\Gamma=0 \tag{2}$$

where $\mathbf{b}$ is the body force, $\mathbf{t}^{a}$ is the applied traction, $\boldsymbol{\varepsilon}^{a}$ are the external strains.

The region Ω is subdivided into a finite number of subdomains (elements), Ω_i, and each region is defined by a finite number of points (nodes). Over these elements, the approximations for $\boldsymbol{\sigma}$, $\mathbf{u}$, and $\boldsymbol{\varepsilon}$ along with their respective variations are

$$\boldsymbol{\sigma}=\mathbf{S}\mathbf{s};\ \delta\boldsymbol{\sigma}=\mathbf{S}\delta\mathbf{s} \tag{3 a, b}$$

$$\boldsymbol{\varepsilon}=\mathbf{E}\mathbf{e};\ \delta\boldsymbol{\varepsilon}=\mathbf{E}\delta\mathbf{e} \tag{4 a, b}$$

$$\mathbf{u}=\mathbf{N}\mathbf{d};\ \delta\mathbf{u}=\mathbf{N}\delta\mathbf{d} \tag{5 a, b}$$

where $\mathbf{S}$ and $\mathbf{E}$ are the stress and strain interpolation functions, $\mathbf{s}$ and $\mathbf{e}$ are nodal point parameters, $\mathbf{N}$ are the shape functions, and $\mathbf{d}$ is the vector of nodal point displacements. Substituting eqns. (3) – (5) into eqn. (2) and noting that the variations $\delta\mathbf{s}$, $\delta\mathbf{e}$, and $\delta\mathbf{d}$ are arbitrary, the following three equations result,

$$\int_{\Omega_i}\left(\mathbf{E}^{T}\mathbf{D}\mathbf{E}\mathbf{e}-\mathbf{E}^{T}\mathbf{D}\boldsymbol{\varepsilon}_{0}+\mathbf{E}^{T}\boldsymbol{\sigma}_{0}-\mathbf{E}^{T}\mathbf{S}\mathbf{s}\right)d\Omega=0 \tag{6}$$

$$\int_{\Omega_i}\left(\mathbf{S}^{T}\mathbf{L}\mathbf{N}\mathbf{d}-\mathbf{S}^{T}\mathbf{E}\mathbf{e}-\mathbf{S}^{T}\boldsymbol{\varepsilon}^{a}\right)d\Omega=0 \tag{7}$$

$$\int_{\Omega_i}\left(\mathbf{L}\mathbf{N}^{T}\mathbf{S}\mathbf{s}-\mathbf{N}^{T}\mathbf{b}\right)d\Omega-\int_{\Gamma_i}\left(\mathbf{N}^{T}\boldsymbol{\sigma}^{a}\right)d\Gamma=0 \tag{8}$$

The following are defined,

$$\mathbf{H}\equiv\int_{\Omega_i}\mathbf{E}^{T}\mathbf{D}\mathbf{E}\,d\Omega;\ \mathbf{A}\equiv\int_{\Omega_i}\mathbf{S}^{T}\mathbf{E}\,d\Omega;\ \mathbf{G}\equiv\int_{\Omega_i}\mathbf{S}^{T}\mathbf{L}\mathbf{N}\,d\Omega \tag{9a, b, c}$$

$$\mathbf{Q}\equiv\int_{\Omega_i}\mathbf{S}^{T}\boldsymbol{\varepsilon}^{a}\,d\Omega;\ \mathbf{f}\equiv\int_{\Omega_i}\mathbf{N}^{T}\mathbf{b}\,d\Omega+\int_{\Gamma_i}\mathbf{N}^{T}\boldsymbol{\sigma}^{a}\,d\Gamma;\ \mathbf{f}_{0}\equiv\int_{\Omega_i}\left(\mathbf{E}^{T}\mathbf{D}\boldsymbol{\varepsilon}_{0}-\mathbf{E}^{T}\boldsymbol{\sigma}_{0}\right)d\Omega \tag{10a, b, c}$$

By substitution of the above definitions, eqns. (6) – (8) become

$$\begin{bmatrix}\mathbf{H} & -\mathbf{A}^{T} & 0\\ -\mathbf{A} & 0 & \mathbf{G}\\ 0 & \mathbf{G}^{T} & 0\end{bmatrix}\cdot\begin{bmatrix}\mathbf{e}\\ \mathbf{s}\\ \mathbf{d}\end{bmatrix}=\begin{bmatrix}\mathbf{f}_{0}\\ \mathbf{Q}\\ \mathbf{f}\end{bmatrix} \tag{11}$$

If A is invertible[1], elimination of **e** and **s** yields

$$\mathbf{G}^{\mathrm{T}}\mathbf{A}^{-\mathrm{T}}\mathbf{H}\mathbf{A}^{-1}\mathbf{G}\mathbf{d} = \mathbf{f} + \mathbf{G}^{\mathrm{T}}\mathbf{A}^{-\mathrm{T}}\mathbf{f}_0 + \mathbf{G}^{\mathrm{T}}\mathbf{A}^{-\mathrm{T}}\mathbf{H}\mathbf{A}^{-1}\mathbf{Q} \tag{12}$$

Stiffness matrix

The stiffness matrix is the coefficient on **d** in eqn. (12). The element is transformed from its global curvilinear coordinates, [x, y], into local linear coordinates, [ξ, η], where $-1 \le \xi \le 1$, and $-1 \le \eta \le 1$. The interpolation functions for a 4 node plane element are chosen to be the following [17]

$$\mathbf{N} = \begin{bmatrix} N_1 & 0 & N_2 & 0 & N_3 & 0 & N_4 & 0 \\ 0 & N_1 & 0 & N_2 & 0 & N_3 & 0 & N_4 \end{bmatrix} \tag{13}$$

$$\mathbf{S} = \mathbf{E} = \begin{bmatrix} 1 & \xi & \eta & 0 & 0 & 0 & 0 & 0 & 0 \\ 0 & 0 & 0 & 1 & \xi & \eta & 0 & 0 & 0 \\ 0 & 0 & 0 & 0 & 0 & 0 & 1 & \xi & \eta \end{bmatrix} \tag{14}$$

where the nodal shape functions are

$$N_I = \frac{1}{4}(1+\xi_I\xi)(1+\eta_I\eta) \tag{15}$$

The elastic moduli matrices for plane stress and plane strain respectively are

$$\mathbf{D} = \frac{E}{1-\nu^2}\begin{bmatrix} 1 & \nu & 0 \\ \nu & 1 & 0 \\ 0 & 0 & \dfrac{1-\nu}{2} \end{bmatrix};\ \mathbf{D} = \frac{E(1-\nu)}{(1+\nu)(1-2\nu)}\begin{bmatrix} 1 & \dfrac{\nu}{1-\nu} & 0 \\ \dfrac{\nu}{1-\nu} & 1 & 0 \\ 0 & 0 & \dfrac{1-2\nu}{2(1-\nu)} \end{bmatrix} \tag{16a,b}$$

where E is the equivalent Young's modulus and ν is Poisson's ratio. By substitution of eqns. (13) – (16) into eqn. (9) the stiffness matrix is formed and integrated symbolically in the computational software package Maple V Release 4 [18].

Load Vector

The load vector is the left-hand side of eqn. (12). It includes terms for body forces, initial stress and strain, and externally applied stress and strain. The externally applied

[1] See [16] for conditions on the invertability of **A**. In this work, the conditions are satisfied and **A** is invertable.

strain field, ε^a, is assumed to be due to a small crack on the element edge. The other terms in the load vector are given standard treatment and are integrated symbolically in Maple V as with the stiffness matrix.

Shown in Fig. 1, the externally applied strain field is due to a small crack embedded in an infinite elastic plate subjected to the far field stresses σ_0, σ_1, and τ_0. The applied strain field is the strain in the adjacent element due only to the presence of the crack on its edge.

The strain field in the plate subject to the far field stresses shown is determined by introducing a complex stress function Z(z), where $z = \xi + i\eta$ and $i = \sqrt{-1}$ [19],

$$\mathrm{Z}(z) = \frac{z}{\sqrt{z^2 - a^2}} \;;\; Z'(z) = \frac{-a^2}{\left(z^2 - a^2\right)^{\frac{3}{2}}} \tag{17}$$

where a is the half crack width.

By superposition of the Mode I and Mode II stresses, the stresses in the plate are

$$\sigma_{\xi\xi} = \sigma_0\left(\mathrm{Re}(Z) - \eta\,\mathrm{Im}(Z')\right) + \sigma_1 + \tau_0\left(2\,\mathrm{Im}(Z) + \eta\,\mathrm{Re}(Z')\right) \tag{18}$$

$$\sigma_{\eta\eta} = \sigma_0\left(\mathrm{Re}(Z) + \mathrm{Im}(Z')\right) + \tau_0\left(-\eta\,\mathrm{Re}(Z')\right) \tag{19}$$

$$\tau_{\xi\eta} = -\sigma_0\eta\,\mathrm{Re}(Z') + \tau_0\left(\mathrm{Re}(Z) - \eta\,\mathrm{Im}(Z')\right) \tag{20}$$

where Re and Im denote the real and imaginary parts.

Using the elasticity relations for plane stress and plane strain, the strain field in the plate is calculated. Far field strains analogous to the far field stress are defined as ε_0, ε_1, and γ_0. The strain in the vicinity of the crack, due only to the presence of the crack, is the total strain field around the crack minus the far field strain given by

$$\varepsilon^a = \begin{Bmatrix} \varepsilon_{\xi\xi} - \left(\varepsilon_0 + \varepsilon_1\right) \\ \varepsilon_{\eta\eta} - \varepsilon_0 \\ \varepsilon_{\xi\eta} - \gamma_0 \end{Bmatrix} \tag{21}$$

This strain field is inserted into eqn. (10a) and integrated numerically with Gauss Quadrature and the complete load vector is assembled. By assuming superposition of the strains given by eqn. (21), additional cracks can be placed on each of the element edges by summing the load vector over the number of edge cracks[2]. This allows for the insertion of a crack at each element interface in the mesh so that each element would have at least one edge crack and at most four.

[2] This assumes that additional cracks in the plate in Fig. 1 can be treated independent of each other.

Interface Failure

To allow for discrete fracture, each element is defined by unique node numbers and displacement continuity is enforced across each element interface until the interface crack fails. While many criteria may be chosen for the failure of the interface crack, it is a simple matter to apply elastic plastic fracture mechanics as shown below.

First it is assumed that the strain energy release rate, G, is a function of the interface crack size. A common form of the curve is an exponential of the form

$$G = \lambda\left(a - a_0\right)^n + R_1 \tag{22}$$

where λ, R_1, and n are material parameters and a_0 is the initial crack half width. The local strain energy release rate at the interface crack is calculated as follows

$$G = \frac{K_I{}^2 + K_{II}{}^2}{E} = \frac{\left(\sigma_0\sqrt{\pi a}\right)^2 + \left(\tau_0\sqrt{\pi a}\right)^2}{E} \tag{23}$$

where the far field Mode I and Mode II stresses, σ_0 and τ_0, are the average of the stresses from the two elements that are adjacent to the interface crack. Equation (22) can be inverted to give the change in crack length as follows

$$\Delta a = \left(a - a_0\right) = \left(\frac{G - R_1}{\lambda}\right)^{\frac{1}{n}} \tag{24}$$

The change in crack length is calculated based on the calculated strain energy release rate at each interface. If the new crack length is greater than the previous crack length, the interface crack grows. If this growth causes the crack width to exceed the interface width, the interface fails and displacement continuity across the interface is no longer enforced.

MECHANICALLY COUPLED COOK OFF EXPERIMENT

A cartoon of the MCCO experiment performed by Dickson et al. [20] is shown in Fig. 2. A small flat cylinder of the high explosive (HE) PBX 9501 is confined in a metal ring of copper. The HE and ring assembly is confined between a window at the top and a solid metal surface at the bottom. The HE specimen has an outer diameter of 25 mm and an inner diameter of 3.175 mm. To simulate the cook-off event, the cylinder of HE is heated uniformly from both the top and bottom to a temperature below the auto-ignition temperature, at which point ignition is initiated at the inner surface of the cylinder by means of an electrically heated NiCr wire.

Experimental observations are made in several ways including the use of a camera that photographs the HE at intervals of 3 to 5 μsec through the top window. The sequence of photographs presented in Fig. 3 shows the typical behavior of HE in a

MCCO experiment after ignition. The photographs show narrow regions of lumination propagating from the inner surface outward toward the confinement ring. This lumination is caused by the ignition of fresh HE surface behind cracks as they propagate. The photographs show that early in the process there are three narrow cracks starting to propagate outward. As time progresses, much of the HE has started to chemically react and the lumination overwhelms the details of the discrete cracks and branching phenomena observed earlier. It is typically observed that 3 to 4 radial cracks propagate after ignition and that such cracks may subsequently bifurcate.

MECHANICALLY COUPLED COOK OFF SIMULATION

Shown in Fig. 4 is a plane strain model of the copper confinement ring and the PBX 9501. The PBX 9501 consists of 1200 discrete fracture elements described above. The element dimensions vary from 0.24 mm x 0.17mm on the inner surface to 0.87 mm x 1.33 mm at the copper ring. The confinement ring consists of 180 standard plane strain elements. The interface between the copper and the HE is modeled as a perfect bond so that the interface is allowed to deform, but no relative motion between the HE and the copper is allowed.

The copper used in the experiment is oxygen free copper. An isotropic elastic plastic material model was used to model the response of the copper. The material has an elastic modulus of 117×10^9 Pa and a Poisson's ratio of 0.33. The stress vs. plastic strain was obtained using a power law model with a yield stress of 65 MPa, a strain hardening exponent of 0.2 and a yield stress coefficient of 292 MPa. The coefficient of thermal expansion (CTE) of copper is a constant 16.56×10^{-6}/°C and the density is 8.9×10^3 kg/m^3.

A material model developed by Hackett and Bennett [21] called ViscoSCRAM is used to model the mechanical and thermal behavior of the explosive. The mechanical behavior is characterized by a viscous model coupled with a damage model so that it is rate dependent but loses strength with the buildup of stress. The thermal behavior includes both mechanical work and chemical decomposition of the explosive. The material properties of importance for the explosive are the constant CTE of 55×10^{-6}/°C and the density of 1.849×10^3 kg/m^3. For the conditions of the experiment it is likely that the material properties are not constant. However, for the present analysis, they are taken to be constant throughout the entire temperature range.

For the discrete fracture model, each element interface in the explosive has been seeded with a small crack. The size of these interface cracks is randomly distributed throughout the mesh according to an approximately flat distribution such that the largest crack is approximately 90% of the smallest element width and the smallest crack is approximately 10% of the smallest element width. This type of definition allows for the failure conditions for fracture to be different for each interface. Also, by choosing several different sets of samples to represent the same flat distribution

and mean crack size, the relationship between the general features of the results and any particular set of interface cracks can be ascertained.

The fracture properties of PBX 9501 have been estimated based on the limited information that is available for HE. The parameters from eqn. (22) are $\beta = 2.0$, $\gamma = 0.1$, and $\lambda = 0.0$.

The interface failure criteria have been modified for this simulation to exclude shear contributions. This is partially due to the difficulties in modeling shear deformation with bilinear finite elements. This difficulty, coupled with the extremely low fracture toughness of PBX 9501, tends to cause prediction of disperse shear cracking that is inconsistent with experimental results. Because the deformation in the experiment is dominated by primarily Mode I type loading, it is felt that this exclusion will not cause significant error in modeling.

To reproduce the conditions of the experiment, the analysis simulated heating from room temperature at a rate of 0.6 °C/sec for 200 seconds. After this initial phase, a pressure of 5 MPa/μsec is applied to the inner surface of the explosive to simulate the rapid pressurization caused by the ignition in the cavity. This internal pressure causes a tangential stress to develop in the explosive and, as a result, cracks begin to open. As these cracks open, the pressure applied to the inner surface is also instantly applied to the crack faces.

RESULTS

During the heat-up phase of the experiment, both the confinement ring and the explosive thermally expand. Because the CTE of PBX 9501 is greater than that of copper, the copper ring serves as a restraint to the expansion of the explosive. At the end of the heating phase, the tensile tangential stress in the copper ring has exceeded the material's yield strength. The compressive tangential stresses in the explosive have caused enough damage that the inner row of elements no longer supports as much stress as the next row of elements.

After the heat-up, a pressure of 5MPa/μsec is applied to the inside of the explosive. As this pressure is applied, it is likely that the inner row of elements is further damaged to the point that they can no longer support tensile stresses, therefore never satisfy the interface failure criterion. However, the stresses in the second (from the inner surface) row of elements transitions to tension. This tension creates strain energy that causes the interface cracks to eventually fail. Shown in Fig. 5 is a graphic of a typical simulation in which many small discrete fractures appear early in the simulation. While the random nature of the interface crack sizes produces some variability in the results, different sets of samples with the same distribution and mean crack size produces generally the same results.

As cracks fail and open up, tensile stresses in the vicinity of the crack are relieved, thereby reducing the strain energy in nearby elements. In addition to relieving nearby

tensile stresses, these discrete cracks also create large stress concentrations in front of the crack, encouraging further growth in the radial direction. Crack growth is further encouraged by the application of the internal pressure to the crack faces, which increases the tensile stress acting on the crack. As simulation time progresses, some of these small cracks will continue to propagate radially outward and some will arrest. In all of the simulations run to date, 3 to 5 large cracks appear and propagate from near the inner surface to near the copper confinement ring with several smaller arrested cracks. Shown in Fig. 6 are the final deformed shapes of four simulations. Each model is the same except that different sets of random crack sizes, with the same distribution and mean size, has been used to seed the element interfaces. The models show that 3 to 5 large cracks appear and propagate out toward the copper ring. In addition to reproducing the fracture patterns, the total simulation time is similar in all cases with the times relative to the end of the heat-up phase being: a) 27.4 μsec, b) 26.9 μsec, c) 29.0 μsec, and d) 28.8 μsec.

SUMMARY AND CONCLUSIONS

A finite element model of the Mechanically Coupled Cook Off experiment conducted on PBX 9501 has been developed. Photographs from the experiment show the formation of 3 to 5 large discrete cracks that propagate from the inner surface radially outward toward the confinement ring. The finite element model developed to simulate the experiments includes the behaviors thought to be essential to modeling the observed behavior. One key component of the numerical model is a discrete fracture model which models macroscopic fracture based upon standard fracture criteria. Although much is still not known about the behavior of PBX 9501, the incorporation of this model with other finite element modeling techniques has produced a model of the MCCO that reproduces the photographic observations of the experiment.

REFERENCE LIST

(1) Liebowitz, H., Sandhu, J. S., Lee, J. D., Menandro, F. C. M., *Eng. Fract. Mech.,* Vol. 50, 1995, pp. 653-670.

(2) Aliabadi, M. H., ed., *Dynamic Fracture Mechanics*, Computational Mechanics Publications, Boston, 1995.

(3) Nishioka, T. *Int. J. Fract.,* Vol. 86, 1997, pp. 127-159.

(4) De Borst, R., *Int. J. Fract.,* Vol. 86, 1997, pp. 5-36.

(5) Banks-Sills, L., Sherman, D., *Int. J. Fract.,* Vol. 41, 1989, pp. 177-196.

(6) Lotfi, H. R., Shing, P. B., *Int. J. Numer. Meth. Eng.,* Vol. 38, 1995, pp. 1307-1325.

(7) Nishioka, T. Stonesifer, R. B., Atluri, S. N., *Eng. Fract. Mech.*, Vol. 15, 1981, pp. 205-218

(8) Li, F. Z., Shih, C. F., Needleman, A., *Eng. Fract. Mech.*, Vol. 21, 1985, pp. 405-421.

(9) Parks, D. M., *Int. J. Fract.*, Vol. 10, 1974, pp. 487-502.

(10) Lemaitre, J., *Eng. Fract. Mech.*, Vol. 25, 1986, pp. 523-537.

(11) Hoff, R., Rubin, C.A., Hahn, G.T., *Eng. Fract. Mech.*, Vol. 23, 1986, pp. 105-118.

(12) Liaw, B. M., Kobayashi, A. S., Emery, A. F., *Int. J. Numer. Meth. Eng.*, Vol. 20, 1984, pp. 967-977.

(13) Xu, X. P., Needleman, A., 1994, *J. Mech. Phys. Solids*, Vol. 42, pp. 1397-1434.

(14) Gerken, J.M., *An Implicit Finite Element Method for Discrete Dynamic Fracture*, MS Thesis, Colorado State University, 1998.

(15) ABAQUS/Standard, Version 5.8, Hibbit, Karlsson and Sorenson Inc.

(16) Weissman, S. L., Taylor, R. L., *Int. J. Numer. Meth. Eng.*, Vol. 33, 1992, pp. 131-141.

(17) Bennett, J. G., Personal Communication, 1997.

(18) Maple V Release 4, Version 4.00f, Waterloo Maple Inc.

(19) Anderson, T. L., *Fracture Mechanics: Fundamentals and Applications, 2nd Edition*, CRC Press, New York, 1995.

(20) Dickson, P.M., Asay, B.W., Henson, B.F., and Fugard, C.S., Observation of the Behavior of Confined PBX 9501 following a Simulated Cookoff Ignition, *Proceedings of the 11th International Symposium on Detonation*, Office of Naval Research, Washington, D.C., 1998.

(21) Hackett, R.M., and Bennett, J.G, *An Implicit Finite Element Material Model for Energetic Particulate Composite Materials*, Los Alamos National Laboratory, Technical Report, LA-UR-99-3139, Los Alamos, New Mexico, 1999.

Figure 1. Crack in an infinite plate on the edge of a 2-D solid element

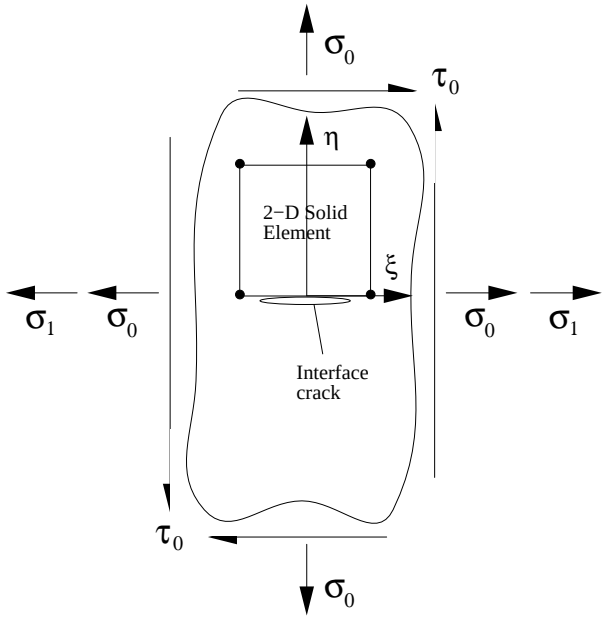

Figure 2. Setup of MCCO experiment.

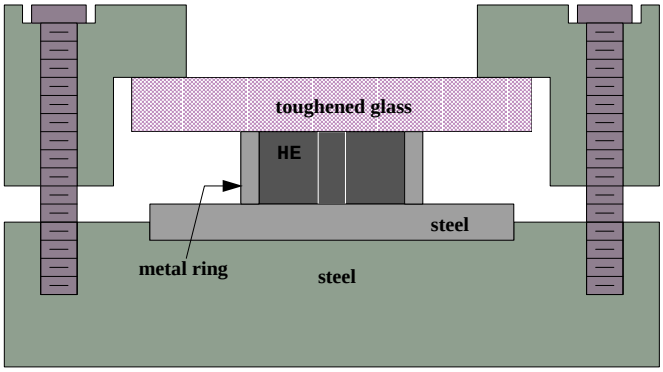

Figure 3. Optical photographs of MCCO experiment.

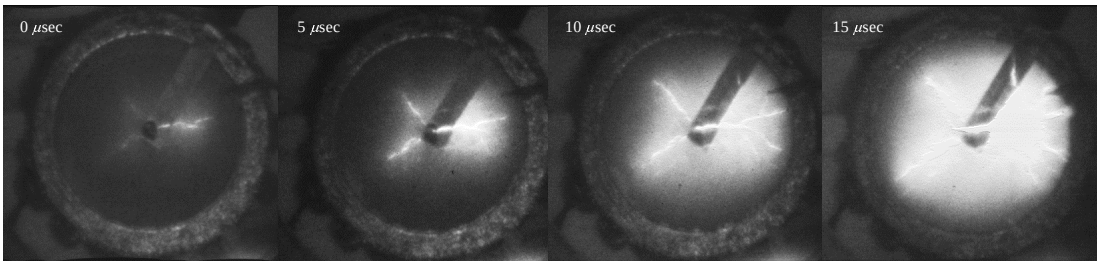

Figure 4. Mesh of the MCCO experiment.

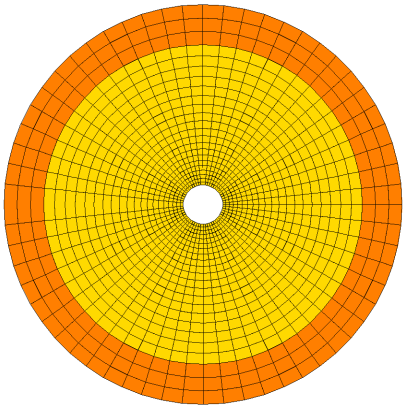

Figure 5. Many small cracks appear early in the simulation. 10x displacement.

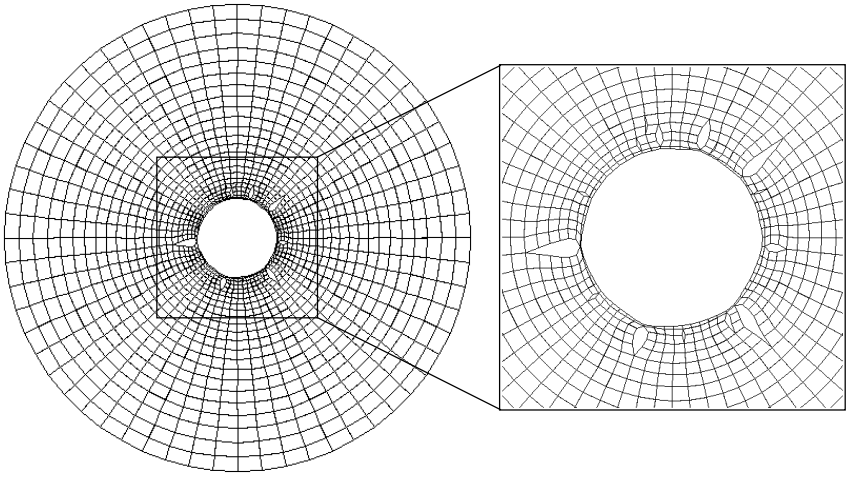

Figure 6. Several simulations show the appearance of 3 to 5 large cracks.